Available online at www.sciencedirect.com
ScienceDirect
Physics Procedia 1 (2008) 467–472
Physics Procedia
www.elsevier.com/locate/procedia

Proceedings of the Seventh International Conference on Charged Particle Optics

# First-order focusing and energy resolution optimization of a biased paracentric hemispherical spectrograph

Omer Sise[a], T.J.M. Zouros[b,c]*, Melike Ulu[a], Mevlut Dogan[a]

[a]*Department of Physics, Science and Arts Faculty, Afyon Kocatepe University, 03200, Afyonkarahisar, Turkey*
[b]*Department of Physics, University of Crete, P.O. Box 2208, 71003 Heraklion, Crete, Greece*
[c]*Institute of Electronic Structure and Laser, P.O. Box 1527, 71110 Heraklion, Crete, Greece*

Received 9 July 2008; received in revised form 9 July 2008; accepted 9 July 2008

**Abstract**

The focusing properties and energy resolution of a hemispherical deflector analyzer (HDA) with a mean radius $R$ = 101.6 mm and large electrode inter-radial distance $\Delta R = R_2 - R_1$ = 58.4 mm is investigated as a function of entry position $R_0$ and bias $\tilde{V}_0 \equiv \tilde{V}(R_0)$. Electron optics simulations show that impressive improvements in energy resolution can be attained for particular empirically determined combinations of $R_0$ and $\tilde{V}_0$ values far from the conventional HDA entry values of $R_0 = \overline{R}$ and $\tilde{V}_0 = 0$, *without the use of any type of fringing field correctors*. This behaviour is a direct result of the lensing properties of the strong fringing fields at the HDA entry, hitherto unexplored, which can be used to restore or even improve the first order focus conditions in a controlled way as shown here. 

*PACS:* 41.85.Ne

*Keywords:* Electron energy analyzer; Electron spectroscopy; Hemispherical deflector analyzers; Electron optics; SIMION

## 1. Introduction

Strong fringing fields at the entry and exit of HDAs with large inter-radial electrode separation $\Delta R \equiv (R_2 - R_1)$ are known to be particularly deleterious to 180° first-order focusing conditions, one of the central advantages of the ideal $1/r^2$-field HDA. The exit radial width $\Delta r_\pi$ in such an HDA is seen in Fig. 1 (top) to become particularly defocused, leading to a corresponding drastic deterioration in its energy resolution. Thus, various fringing field corrector schemes are traditionally applied to reduce as much as possible this defocusing and restore ideal field behaviour [1].

Recently, Benis & Zouros [2] showed in simulation that the energy resolution of an HDA could be improved for particular combinations of values of $R_0$ *smaller* than $\overline{R}$, and *positive* entry bias $\tilde{V}_0 > 0$ (see Fig. 1 middle) relative to the conventional entry HDA for which $R_0 = \overline{R}$ and $\tilde{V}_0 = 0$ (see Fig. 1 top). This type of HDA was termed a *biased*

* Corresponding author. Tel.: +30-2810-394117
*E-mail address*: tzouros@physics.uoc.gr

doi:10.1016/j.phpro.2008.07.128

*paracentric* HDA. A *real* (not simulated) positively biased paracentric HDA using a four element zoom lens and position sensitive detector (PSD), has been successfully applied to zero-degree Auger projectile electron spectroscopy in energetic ion-atom collisions [3,4] with excellent resolution (≤0.1%). While the reason for this resolution improvement is still not completely understood, it was recently shown that *no* such improvement can be expected from the *ideal* positively biased paracentric HDA [5]. In fact, for this HDA both $\Delta r_\pi$ and the corresponding base energy width $\Delta E_B$ are slightly worse than that of the *ideal* conventional HDA [6,7]. It is clear that the strong fringing fields in the paracentric HDA must therefore be somehow responsible.

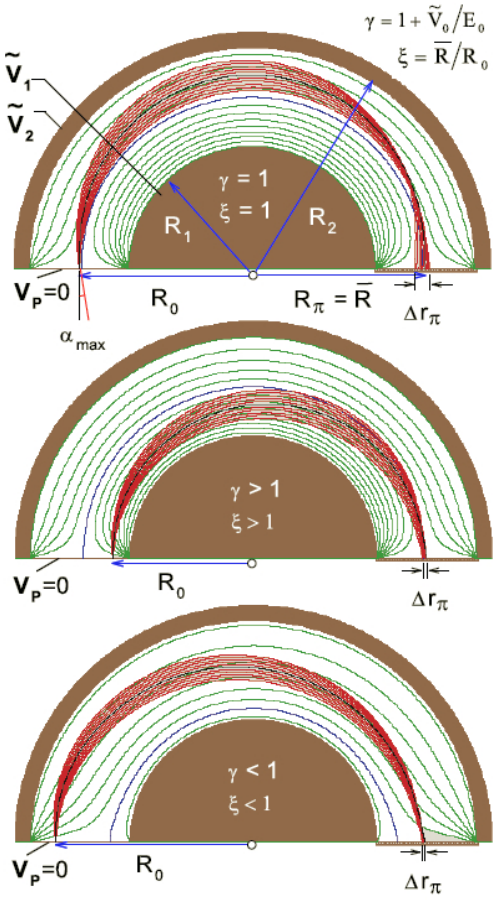


Fig. 1. (Colour online.) SIMION [8] simulations of electron trajectories in an HDA with $R_1$ = 72.4 mm, $R2$ = 130.8 mm ($\overline{R}$ = 101.6 mm) and electrode voltages $\tilde{V}_1$, $\tilde{V}_2$ set according to Eq. (1) for pass energy $E_0$ = 1000 eV. Strong fringing fields are evident from the equipotentials, shown in green, plotted every 100V. The blue line is the equipotential for 0V. Top: Conventional HDA with unbiased ($\gamma$ = 1) central ($\xi$ = 1) entry. Middle: Positively biased paracentric HDA with $\gamma > 1$ and $\xi > 1$. Bottom: Negatively biased paracentric entry with $\gamma < 1$ and $\xi < 1$. The two paracentric entries demonstrate much improved focusing at the 180° detection plane, due to the strong lensing effect of the fringing fields.

In this presentation, we show via electron optics simulations using SIMION [8], that the energy resolution of an HDA is also improved for new *negative* bias $\tilde{V}_0 < 0$ values for which $R_0 > \overline{R}$ [7], as shown in Fig. 1 (bottom). A methodical search for the optimal combinations of $R_0$ and $\tilde{V}_0$ values minimizing $\Delta r_\pi$ (and $\Delta E_B$) was performed over the entire range $R_1 < R_0 < R_2$ for both positive and negative values of $\tilde{V}_0$. These new negative bias positions with $R_0 > \overline{R}$ are found to lead to even *smaller* $\Delta r_\pi$ and $\Delta E_B$ (at least for point sources [7]) than the older positive bias entries with $R_0 < \overline{R}$ .

The biased paracentric HDA thus holds the promise of the highest resolution *without the use of any additional field correction schemes* [1], clearly a great practical advantage, particularly for HDAs utilizing a PSD and therefore requiring large $\Delta R$.

## 2. Trajectory and energy resolution calculations

Trajectory calculations using SIMION [8] were performed for electrons ($q = -e = -1.602\times10^{-19}$ C) with energy $E$ and *ideal* field electrode potentials $\tilde{V}_i \equiv \tilde{V}(R_i)$ ($i$ = 1, 2) for the central principal ray pass energy $E_0$ = 1000 eV using the following equation [5,9]:

$$q\tilde{V}_i = E_0\left\{1-\frac{\gamma}{\xi}\left[\frac{D_0}{R_i}-1\right]\right\} \quad (i = 1, 2) \tag{1}$$

$D_0 = R_0\,(1+\xi) = R_0 + R_\pi$ is the range (or dispersion length) of the central ray. The paracentricity, $\xi = \overline{R}/R_0$, characterizes the entry asymmetry of the HDA, while $\gamma$ is a parameter used to determine the value of the ideal field equipotential $\tilde{V}_0$ at the entry radius $R_0$. It is used to control the values of $\tilde{V}_i$ in Eq. (1) and is related to the bias $\tilde{V}_0$ according to the relation [5]:

$$q\tilde{V}_0 = (1-\gamma)E_0 \tag{2}$$

Thus, a conventional HDA is seen to have $\gamma = 1$ ($\tilde{V}_0 = 0$) and $\xi = 1$ ($R_0 = \overline{R}$). In Fig. 1, conventional and paracentric focusing conditions are demonstrated. In Fig. 2, the exit radial base width $\Delta r_\pi$ (see Fig. 1) is plotted as a function of $R_0$ for entry angles $|\alpha| \le \alpha_{max} = 1°$ and various values of the biasing parameter $\gamma$.

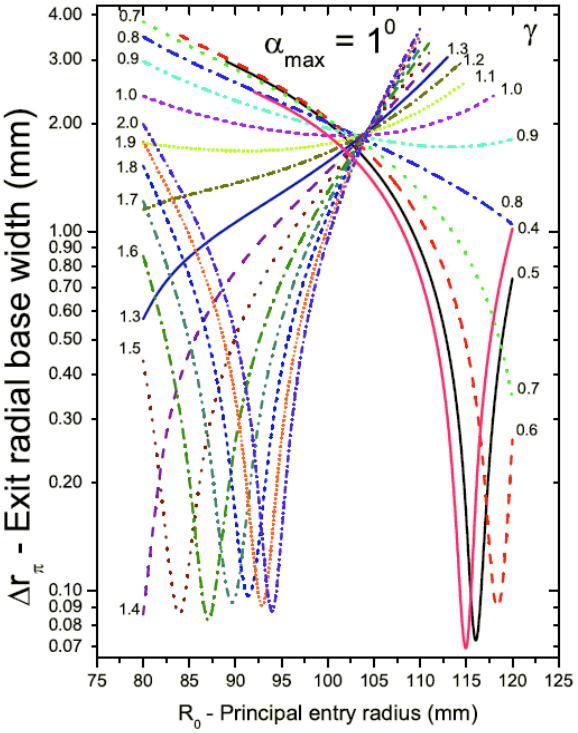


Fig. 2. (Colour online.) Plot of exit radial base width $\Delta r_\pi$ versus $R_0$ for a range of biasing parameter $\gamma$ values ($0.4 < \gamma < 2$) with maximum entry angle $\alpha_{max} = 1°$ and 100% transmission.

Finally, in Fig. 3, $\Delta r_\pi$ has been converted by energy calibration to a base energy width $\Delta E_B$ and the base resolution $\Delta EB/E_0$ is plotted as a function of $R_0$ for typical values of maximum entry angle $\alpha_{max}$ = 1° – 5° and various values of $\gamma$. In both figures, two ranges of strong focusing and much improved energy resolution are observed for which $80 \leq R_0 \leq 95$ mm and $115 \leq R_0 \leq 120$ mm with $\gamma$ in the range of 1.5 and 0.5, respectively. The reliability of our simulations was further checked by repeating critical calculations using higher grid densities λ (gu/mm) with correspondingly higher simulation accuracy [9].

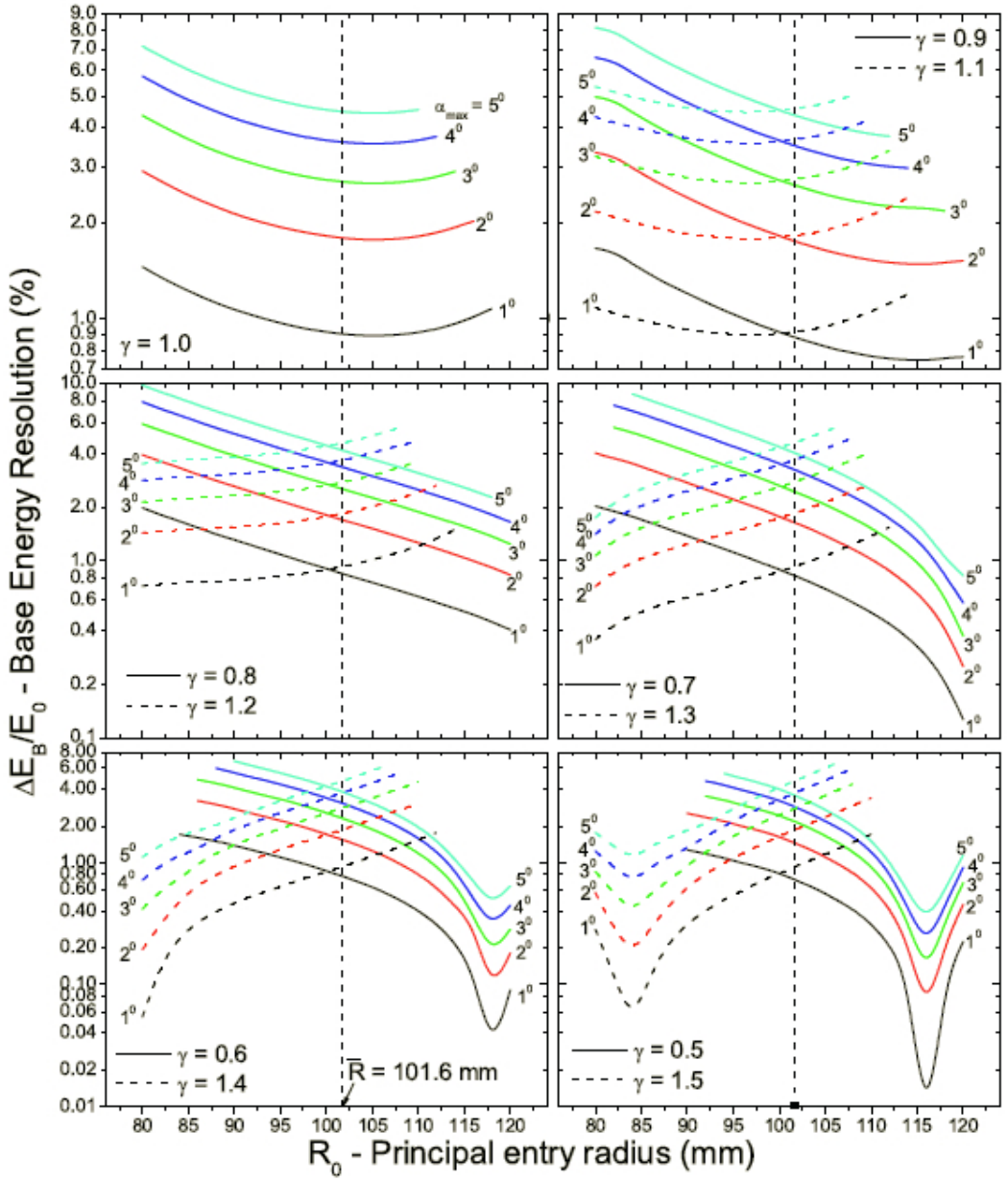


Fig. 3. (Colour online.) Base energy resolution as a function of $R_0$ for $\alpha_{max}$ = 1° – 5°. Lines: $\gamma > 1$ (dashed) and $\gamma \leq 1$ (continuous). Resolution minima are seen near $R_0$ = 82:5 mm for $\gamma \approx 1.5$, and $R_0$ = 116 mm for $\gamma \approx 0.5$.

To further assess the performance of the HDA, line shape simulations were also performed using a Monte-Carlo type approach, in which the entry angle $\alpha$ was randomly sampled with $|\alpha| \leq \alpha_{max}$ for 100,000 monoenergetic electrons emitted from a *point* at $R_0$ with energy $E$. As an example, in Fig. 4 we show the line shape for the fringing field conventional entry HAD ($\gamma = 1$ and $R_0 = 101{:}6$ mm – dashed red line) compared to the same for both positive bias ($R_0 = 82{:}55$ mm and $\gamma = 1{:}5$ – black continuous line) [2,5] and negative bias ($R_0 = 116{:}0$ mm and $\gamma = 0{:}5$ – green dotted line) paracentric HDA at three energies $E/E_0 = 0{:}95$; 1; 1:05 with $\alpha_{max} = 2°$. The line shape for conventional entry in an *ideal* field (blue dash-dot line) is also shown for comparison. Both paracentric entries show a much improved base energy resolution with fairly symmetric line shape compared to the much broader conventional fringing field HDA line shape. Improvement factors for a typical value of $\alpha_{max} = 2°$ can be as large as 35 (=17.976/0.514) for the point source negative bias entry, dropping to a still impressive factor of about 4.2 (=22.741/5.395) for the $\Delta r_0 = 1$ mm source size [7] as shown in Table 1. It is interesting to note that for point source $\Delta r_0 = 0$, the fringing field negative bias paracentric HDA has a smaller $\Delta r_\pi$ than the ideal field case even at the same $R_0$ and $\gamma$, while the positive bias HDA has a larger $\Delta r_\pi$ than the ideal field case. This shows that, for the negative bias case, better focusing than the ideal field case can be achieved. However, for an extended source (e.g. $\Delta r_0 = 1$ mm) this trend is reversed, the positive bias paracentric HDA now having a better focus than the ideal field case. Nevertheless, both fringing paracentric cases are seen to have better resolution than the conventional ($R_0 = \overline{R} = 101{:}6$ mm, $\gamma = 1$) fringing field case, with the negative bias case having the largest relative resolution gain, chiefly due to its larger dispersion length $D_0$. Clearly, the exact resolution will depend on usage and therefore on the specific requirements on $\alpha_{max}$ and $\Delta r_0$.

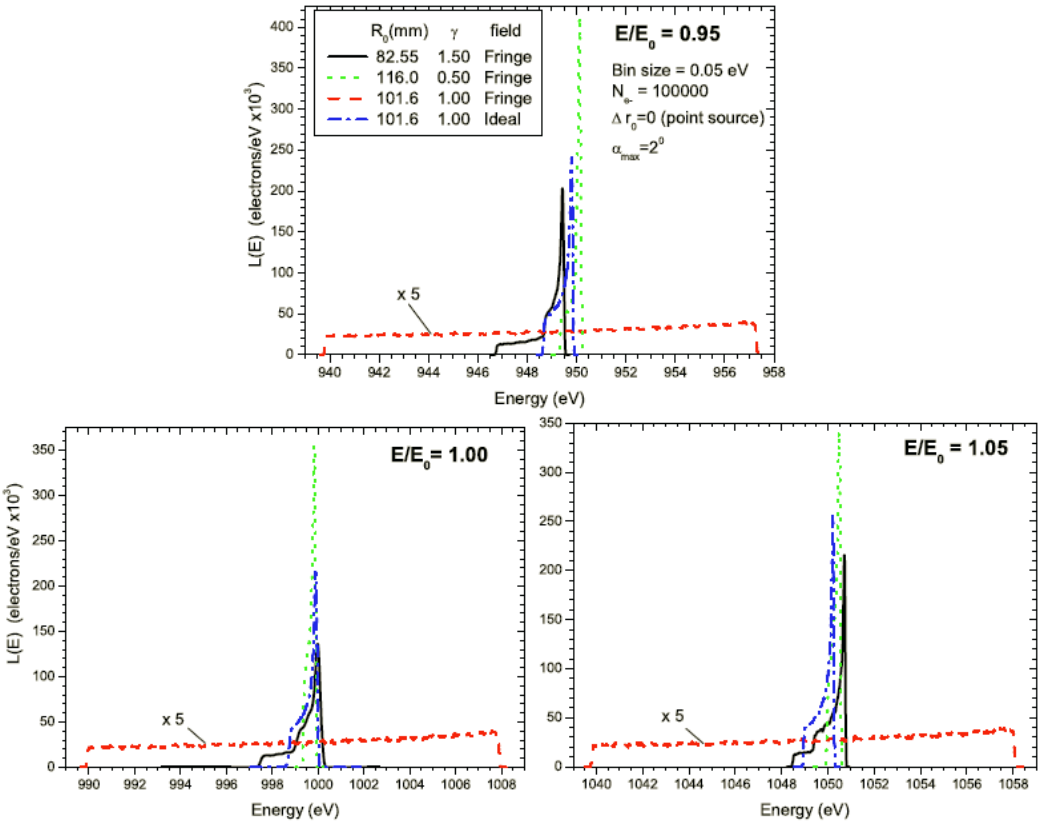


Fig. 4. (Colour online.) Point source line shapes $L(E)$ for electrons with energies $E = (0.95; 1.0; 1.05)\ E_0$, for three different entry configurations of $R_0$ and biasing parameter $\gamma$ with the HDA tuned to the pass energy $E_0 = 1000$ eV. The two biased paracentric entries are seen to result in much improved line shapes relative to those obtained for the conventional (unbiased central entry) HDA.

Table 1
HDA and electron trajectory simulation parameters for pass energy $E_0$ = 1000 eV and $\alpha_{max}$ = 2° for the three cases shown in Fig. 1. Line shape exit radial widths $\Delta r_\pi$ and base energy widths $\Delta E_B$ are tabulated for both point ($\Delta r_0$ = 0 mm) (line shapes shown in Fig. 4) and extended source ($\Delta r_0$ = 1 mm) (line shapes shown in Ref. [7]) and compared to those for the ideal field. Central ray ($\alpha$ = 0) exit radii $r_\pi$ are also compared.

| | | HDA parameters | | | | Electron trajectory results | | | | |
|---|---|---|---|---|---|---|---|---|---|---|
| Fig. 1 | Field | Independent | | Dependent | | Central Ray | $\Delta r_0$ = 0 mm | | $\Delta r_0$ = 1 mm | |
| | | $R_0$ (mm) | $\gamma$ | $\xi$ | $\tilde{V}_0$ (V) | $r_\pi$ (mm) | $\Delta r_\pi$ (mm) | $\Delta E_B$ (eV) | $\Delta r_\pi$ (mm) | $\Delta E_B$ (eV) |
| | Ideal[a] | 101.6 | 1 | 1 | 0 | 101.6 | 0.247 | 1.218 | 1.245 | 6.135 |
| | Ideal[a] | 82.55 | 1.5 | 1.231 | +500 | 101.6 | 0.276 | 1.827 | 1.273 | 8.437 |
| | Ideal[a] | 116.0 | 0.5 | 0.8759 | –500 | 101.6 | 0.232 | 0.609 | 1.230 | 3.232 |
| top | Fringe[b] | 101.6 | 1 | 1 | 0 | 101.166 | 3.683 | 17.976 | 4.657 | 22.741 |
| middle | Fringe[b] | 82.55 | 1.5 | 1.231 | +500 | 101.726 | 0.403 | 2.596 | 1.074 | 6.901 |
| bottom | Fringe[b] | 116.0 | 0.5 | 0.8759 | –500 | 100.572 | 0.160 | 0.514 | 1.680 | 5.395 |

[a] Theory: Non-relativistic calculation based on Eq. (99) of Ref. [5] as shown in Ref. [6].
[b] SIMION: Simulation results for grid density $\lambda$ = 10 gu/mm, heavy electron mass $m = 10^{12}\, m_e$, $R_2$ with −1 gu correction as discussed in Ref. [9].

We have demonstrated the utility of using the lensing properties of the strong fringing fields of an HDA to improve its energy resolution *without the use of any additional fringing field corrector electrodes*. Further exploration of the lensing properties of the strong fringing fields at the entry of particle spectrometers and the extent to which they can be used to improve the charged particle optics characteristics of these devices is clearly of interest.

## Acknowledgements

We would like to thank D. Dahl and D. Manura for helpful communications regarding the use of SIMION. This work was supported by the State Planning Organization in Turkey, through grant 2002K120110 and Afyon Kocatepe University, Scientific Research Project Commission, through grant 031-FENED-07, and a travel grant by ELKE-University of Crete.

## References

[1] Omer Sise, T.J.M. Zouros, Melike Ulu and M. Dogan, Proceedings of CPO-7 Conference (this volume).
[2] E.P. Benis and T.J.M. Zouros, Nucl. Instrum. Methods Phys. Res. A 440 (2000) 462.
[3] E.P. Benis *et al.*, Nucl. Instrum. Methods Phys. Res. B 146 (1998) 120.
[4] E.P. Benis, T.J.M. Zouros, T.W. Gorczyca, A.D. Gonzalez and P. Richard, Phys. Rev. A 69 (2004) 052718.
[5] T.J.M. Zouros and E.P. Benis, J. Electron Spectrosc. and Relat. Phenom. 125 (2002) 221; *ibid.* 142 (2005) 175.
[6] T.J.M. Zouros, J. Electron Spectrosc. and Relat. Phenom. 152, 67-77 (2006); *ibid.* in print (2006).
[7] T.J.M. Zouros, Omer Sise, Melike Ulu and Mevlut Do·gan, Meas. Sci. & Tech. submitted (2006).
[8] D.A. Dahl, *SIMION 3D v6.0*, Idaho National Engineering Laboratory, Idaho Falls, 1996.
[9] T.J.M. Zouros, Omer Sise, F.M. Spiegelhalder, D.J. Manura, Int. J. of Mass Spectro. in print (2006).